

Segregation of antiferromagnetism and high-temperature superconductivity in $\text{Ca}_{1-x}\text{La}_x\text{Fe}_2\text{As}_2$

Shanta R. Saha,^{1,*} T. Drye,¹ S. K. Goh,² L. E. Klintberg,² J. M. Silver,² F. M. Grosche,² M. Sutherland,² T. J. S. Munsie,³ G. M. Luke,³ D. K. Pratt,⁴ J. W. Lynn,⁴ and J. Paglione^{1,†}

¹*Center for Nanophysics and Advanced Materials, Department of Physics, University of Maryland, College Park, Maryland 20742, USA*

²*Cavendish Laboratory, University of Cambridge, J.J. Thomson Avenue, Cambridge CB3 0HE, United Kingdom*

³*Department of Physics and Astronomy, McMaster University, 1280 Main Street West, Hamilton, Ontario, Canada L8S 4M1*

⁴*NIST Center for Neutron Research, National Institute of Standards and Technology, Gaithersburg, Maryland 20899, USA*

(Received 25 October 2013; revised manuscript received 4 April 2014; published 23 April 2014)

We report the effect of applied pressures on magnetic and superconducting order in single crystals of the aliovalent La-doped iron pnictide material $\text{Ca}_{1-x}\text{La}_x\text{Fe}_2\text{As}_2$. Using electrical transport, elastic neutron scattering, and resonant tunnel diode oscillator measurements on samples under both quasihydrostatic and hydrostatic pressure conditions, we report a series of phase diagrams spanning the range of substitution concentrations for both antiferromagnetic and superconducting ground states that include pressure-tuning through the antiferromagnetic (AFM) superconducting critical point. Our results indicate that the observed superconducting phase with a maximum transition temperature of $T_c = 47$ K is intrinsic to these materials, appearing only upon suppression of magnetic order by pressure-tuning through the AFM critical point. Thus, the superconducting phase appears to exist exclusively in juxtaposition to the antiferromagnetic phase in a manner similar to the oxygen- and fluorine-based iron-pnictide superconductors with the highest transition temperatures reported to date. Unlike the lower- T_c systems, in which superconductivity and magnetism usually coexist, the tendency for the highest- T_c systems to show noncoexistence provides an important insight into the distinct transition temperature limits in different members of the iron-based superconductor family.

DOI: [10.1103/PhysRevB.89.134516](https://doi.org/10.1103/PhysRevB.89.134516)

PACS number(s): 74.70.Xa, 74.90.+n

I. INTRODUCTION

The interplay between structural, magnetic, and superconducting properties in the newly discovered iron-based superconducting compounds has been a central theme in attempts to elucidate the nature of Cooper pairing in this new family of high-temperature superconductors [1–4]. In particular, manipulation of the electronic structure via chemical substitution or applied pressure is thought to play a key role in the disruption of antiferromagnetic order and the stabilization of superconductivity [2]. These similar but unique tuning parameters generically produce the well-known phase diagram of the iron-based superconductors, with an antiferromagnetic (AFM) ordering temperature T_N continuously suppressed toward zero as a function of doping, substitution, or pressure, before impinging on a superconducting (SC) state with transition temperature T_c that also varies as a function of tuning parameter. The interplay of these two phases has been the focus of much effort in understanding the nature and origin of both ground states.

Experiments have shown a variety of behavior, including both exclusive separation of the AFM and SC phases as well as microscopic coexistence of the two. As first observed in the RFeAsO “1111” oxypnictide compounds [5], which continue to possess the highest T_c values in the entire family, the AFM and SC phases appear to show little to no coexistence as observed in $\text{LaFeAsO}_{1-x}\text{F}_x$ [6], $\text{CeFeAsO}_{1-x}\text{F}_x$ [7], and $\text{SmFeAsO}_{1-x}\text{F}_x$ [8] systems, even exhibiting a first-order-like transition between the two phases. In contrast, most of the intermetallic “122” compounds with the ThCr_2Si_2 crystal structure—such as $\text{BaFe}_{2-x}\text{Co}_x\text{As}_2$

[9–12] and $\text{Ba}_{0.77}\text{K}_{0.23}\text{Fe}_2\text{As}_2$ [13]—exhibit a wide range of microscopic coexistence between AFM and SC phases, which has even been claimed at the atomic level [14]. Interestingly, Ran *et al.* reported that in Co-doped CaFe_2As_2 , superconductivity ($T_c \sim 15$ K) and AFM are phase-separated, and the ground state depends on the details of the thermal processing of the single crystals [15]. While mean-field theories have proven useful in explaining the cooperative competition between AFM and SC transitions and the manner by which the two phases shape the phase diagram of the 122 materials [16–18], the exclusive repulsion of the two phases in the 1111 materials and its relevance to achieving the highest T_c values remains to be understood [19,20].

In the smallest unit cell member of the 122 family, CaFe_2As_2 , AFM order can be suppressed by both chemical substitution (e.g., Co and Ni for Fe [21,22], Na for Ca [23]) and applied quasihydrostatic pressure [24–26] to reveal superconductivity. Interestingly, no bulk superconductivity has been reported in CaFe_2As_2 under hydrostatic pressure [27]. Recently, a new approach was reported to tuning the CaFe_2As_2 phase diagram using rare-earth substitution, utilizing the doping effect of replacing divalent Ca^{2+} with trivalent R^{3+} rare-earth elements (La, Ce, Pr, and Nd) in $\text{Ca}_{1-x}\text{R}_x\text{Fe}_2\text{As}_2$ [28–30], as well as a chemical pressure effect due to the ionic size mismatch between Ca and the light rare earth elements. This approach induces superconductivity with the highest transition temperatures yet reported for the intermetallic iron-based superconductors [31,32], with T_c values reaching as high as 49 K [28–30,33]. However, the lack of a full-volume-fraction SC phase in all R -substituted series has raised questions about the intrinsic nature of superconductivity in this system, which appears in both uncollapsed (for La and Ce) and collapsed (for Pr and Nd) tetragonal states [28]. While the former may be alleviated by recent reports of stronger Meissner

*srsaha@umd.edu

†paglione@umd.edu

screening in phosphorus-substituted samples [34], the latter case is particularly intriguing since the widely believed spin fluctuation pairing mechanism is likely inactive in the collapsed state due to the quenched iron moment [35–38].

Here we report the intrinsic separation of AFM and SC phases in the La-doping series, $\text{Ca}_{1-x}\text{La}_x\text{Fe}_2\text{As}_2$, found by fine-tuning samples with a range of La concentrations through the AFM-SC critical point with applied pressure. We performed electrical resistivity and neutron scattering experiments to investigate this evolution as a function of pressure, utilizing both quasihydrostatic as well as hydrostatic pressure experiments to rule out extrinsic strain effects. With clear evidence of an onset of the superconducting phase upon continuous pressure tuning beyond the AFM ordered phase, we conclude that the superconductivity observed in rare-earth-doped CaFe_2As_2 is intrinsic to the material and does not arise due to an impurity phase. With a resultant phase diagram strikingly similar to that of the 1111 pnictide superconductors, we draw parallels between the two systems and speculate on a common origin of superconductivity with the highest transition temperatures in the iron-based family. Experimental details and organization of the pressure experiments are outlined in Sec. II, followed by discussion of our main results for each pressure experiment in Sec. III and general conclusions in Sec. IV.

II. EXPERIMENTAL DETAILS

Single-crystal samples of $\text{Ca}_{1-x}\text{La}_x\text{Fe}_2\text{As}_2$ were grown using the FeAs self-flux method, [39] yielding crystals as large as $\sim 10 \times 10 \times 0.1 \text{ mm}^3$. Chemical analysis was obtained via both energy-dispersive (EDS) and wavelength-dispersive (WDS) x-ray spectroscopy, showing 1:2:2 stoichiometry between (Ca,La), Fe, and As concentrations. The actual La concentration was determined using WDS and single-crystal x-ray diffraction measurements [28].

Figure 1 presents the La substitution phase diagram for $\text{Ca}_{1-x}\text{La}_x\text{Fe}_2\text{As}_2$, showing the evolution of AFM and SC transition temperatures as determined by magnetic susceptibility and electrical resistivity measurements, respectively. For details, we refer the reader to our previous study [28]. As shown, La substitution suppresses AFM order with the associated structural transition from nonmagnetic tetragonal to orthorhombic phase, noted as magnetostructural transition at temperature T_N , and induces superconductivity with T_c values reaching 40 K in concentrations above 14%. Throughout the range of La substitutions, a second superconducting transition with $T_c \simeq 10 \text{ K}$ is always present in trace forms. This phase is believed to be related to the filamentary superconducting phase [40] induced in CaFe_2As_2 under quasihydrostatic pressure conditions (i.e., a typical liquid-medium clamp cell pressure experiment) [24,25] that is absent under true hydrostatic pressure conditions (i.e., in a helium gas cell) [27]. In the present study, we focus on the high- T_c phase that occurs with T_c values exceeding 30 K, which does not show any traces in samples with $x < 0.14$ under ambient conditions and is believed to be of a different origin. We have chosen three “underdoped” (i.e., $x < 0.14$) samples and one “overdoped” (i.e., $x > 0.14$) sample to investigate under pressure, indicated by the positions of the arrows in Fig. 1.

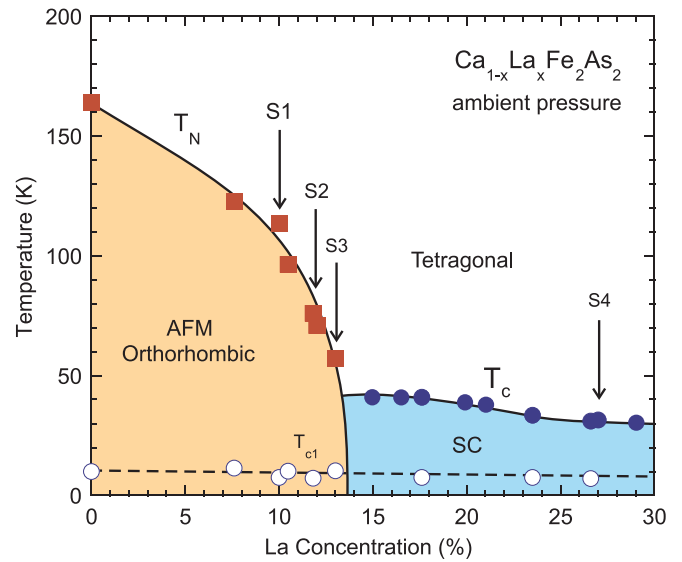


FIG. 1. (Color online) Lanthanum substitution phase diagram of $\text{Ca}_{1-x}\text{La}_x\text{Fe}_2\text{As}_2$, showing the antiferromagnetic (AFM) transitions at T_N (squares) and superconducting transitions (circles). Open circles indicate the “10 K” superconducting transition T_{c1} (see text). Arrows indicate the La concentrations of samples S1, S2, S3, and S4 (with $x = 0.10, 0.12, 0.13$ and 0.27 , respectively) investigated in this study.

The experiments are organized as follows. First, electrical resistivity measurements under quasihydrostatic pressure were carried out at the University of Maryland using the four-wire contact method on sample S1 [$x = 0.10$, $T_N(0) = 114 \text{ K}$], employing a miniature piston-cylinder cell with a maximum pressure range of 15 kbar. The sample was loaded in a Fluorinert liquid pressure medium along with a tin manometer. Increasing pressure was applied systematically after each thermal cycle, with resistance measurements taken on cooling. Pressures were calibrated at low temperature by measuring the resistance of the tin manometer and using the change of its superconducting transition temperature with pressure [41].

Second, hydrostatic pressure experiments were carried out using helium gas pressure systems. Compared with the clamp cell experiment, which employs a liquid pressure medium that solidifies at low temperatures, the use of helium in a gas cell provides the best possible hydrostatic pressure sample environment over a much wider range of temperatures and pressures. In particular, the He freezing point only increases to about 50 K at $P = 0.7 \text{ GPa}$ (7 kbar), allowing the best possible hydrostatic sample environment in our experimental setup.

Neutron diffraction studies under He gas pressure were carried out on sample S2 [$x = 0.12$, $T_N(0) = 70 \text{ K}$] using the BT-4 Filter Analyzer Triple-Axis Spectrometer at the NIST Center for Neutron Research using an Al-alloy He-gas pressure cell to ensure hydrostatic pressure conditions, as reported previously [36]. The cell was connected to a pressurizing intensifier through a high-pressure capillary that allowed continuous monitoring and adjusting of the pressure. Using this system, the pressure could be varied at fixed temperatures above the He solidification line, or temperature could be scanned at nearly constant pressures. A helium reservoir allowed the pressure to remain relatively constant as the temperature was changed.

Electrical resistivity measurements under He gas pressure were carried out at McMaster University on sample S3 [$x = 0.13$, $T_N(0) = 58$ K], measured using a helium gas pressure system as reported previously [27]. The sample was loaded in the pressure cell with a standard four-probe configuration, and cooled in a helium storage dewar, with pressure applied *in situ* by an external helium compressor. The maximum pressure attained was 4 kbar for the helium pressure cell, and we employed a cooling rate of approximately 1 K/min through the structural transitions. To ensure that the applied pressure in the compressor was transmitted to the pressure cells, we always set the pressure while the system temperature was maintained above 70 K, thus avoiding the possibility of helium freezing in the feed capillary.

Finally, quasihydrostatic pressure was applied to overdoped samples [$x = 0.27$, $T_c(0) = 31$ K] at Cambridge University, using both a Moissanite anvil cell to obtain tunnel diode oscillator (TDO) measurements of sample S4, and a miniature piston-cylinder cell with lead manometer (similar to that noted above) to conduct conventional four-wire resistivity measurements of sample S4 (same batch as sample S4). The TDO technique tracks the resonant frequency of an oscillator formed by a tunnel diode (a BD-4 equivalent from MPulse) and a microcoil in the gasket hole of a Moissanite anvil cell [42], using ruby fluorescence spectroscopy for pressure determination. Both pressure cells utilized glycerin as the pressure transmitting fluid.

III. EXPERIMENTAL RESULTS

A. Quasihydrostatic clamp cell

Resistivity measurements of sample S1 [$x = 0.10$, $T_N(0) = 114$ K] were carried out under quasihydrostatic pressures with a piston-cylinder clamp cell using a liquid (Fluorinert) pressure medium, and they are presented in Fig. 2(a). At ambient pressure, the AFM transition with the associated structural transition is indicated by the upward rise of resistivity ρ with decreasing temperature that results in a kink in the temperature derivative $d\rho/dT$ that coincides with the onset of a step in the magnetic susceptibility at $T_N(0) = 114$ K (see the supplemental material [43]). This value of $T_N(0) = 114$ K, suppressed from 165 K in the parent compound, allows for a more accessible range of behavior to be reached in a conventional piston-cylinder clamp cell. Upon application of pressure, the overall resistivity values are suppressed, along with the AFM transition temperatures. Because the distinct onset of AFM order is smeared out as pressure is increased, we define $T_N(P)$ (i.e., the pressure-dependent T_N) to be the temperature below which $d\rho/dT$ deviates from a constant value. This translates to the onset of curvature in the resistivity curves (see the supplemental material [43]), as indicated by the position of the arrows in Fig. 2(a). The lowest detectable trace of T_N is at ~ 65 K at 10.5 kbar, yielding a pressure coefficient of $dT_N/dP \simeq -4.7$ K/kbar for the range $T_N(P)$ between 114 and 65 K. This evolution is shown in the pressure-temperature phase diagram presented in Fig. 2(b).

At low temperatures, a superconducting transition at $T_{c1} \simeq 8$ K, believed to be related to the “10 K” phase noted above, is observable at ambient pressure and does not appear to evolve

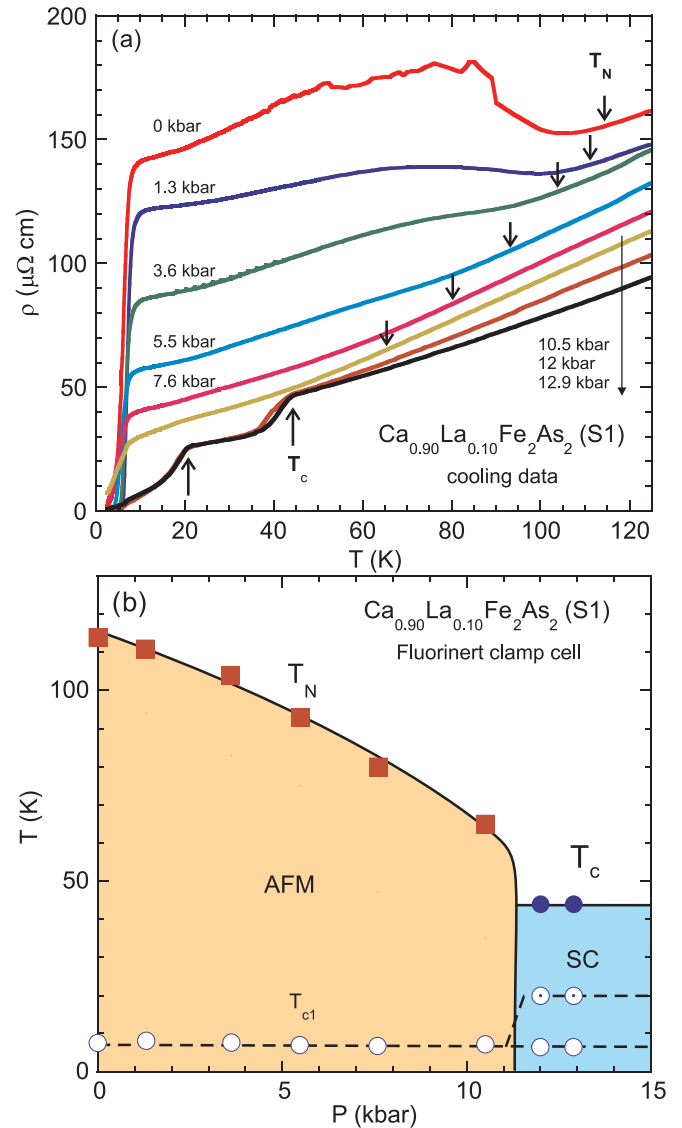


FIG. 2. (Color online) Quasihydrostatic pressure experiment on $\text{Ca}_{0.9}\text{La}_{0.1}\text{Fe}_2\text{As}_2$ (underdoped sample “S1” in Fig. 1) using a piston-cylinder clamp cell with the sample loaded in a Fluorinert liquid pressure medium. (a) Resistivity measured upon cooling temperature as a function of applied pressures. Down arrows indicate the position of the antiferromagnetic ordering temperatures T_N as defined by the kink in $d\rho/dT$ (see text and Fig. 1 of the supplemental material [43]). Up arrows indicate the onset of superconducting transitions, including the high- T_c phase at 44 K, that appear abruptly upon an increase of pressure from 10.5 to 12 kbar. (b) Phase diagram for sample S1, showing the evolution of T_N (squares) and superconducting transition temperatures T_c (closed circles) and T_{c1} (open circles), which is related to the “10 K” phase observed in undoped CaFe_2As_2 at ambient pressure. An intermediate superconducting phase appears above 10.5 kbar near ~ 20 K (dotted circles).

with pressure, as shown in the phase diagram in Fig. 2(b). Increasing pressure to a higher value reveals two features that suddenly emerge as abrupt drops in resistivity at $T_c = 44$ K and $T_{c2} = 20$ K. The dramatic appearance of these features appears to be associated with the suppression of AFM order, as shown in Fig. 2(b): once AFM order is suppressed below the value of

the high transition temperature of 44 K, superconductivity emerges. While the transitions are not complete, the trace of superconductivity is believed to be associated with the same phase that is induced with La substitution, as shown in Fig. 1, and with other rare-earth substitutions [28], suggesting pressure and doping are acting to produce very similar phase diagrams in this range of parameters. The reason for the appearance of two partial transitions (i.e., at 20 and 44 K) is not clear. Upon close inspection of the resistivity data, the signature of T_{c1} near 8 K is still present above the critical pressure where T_N is suppressed, indicating its presence is impervious to any change in the overall ground state of the material. In contrast, the signatures of superconductivity at 20 and 44 K abruptly appear beyond the suppression of AFM phase transition. While we believe the 44 K transition to be unique to the $\text{Ca}_{1-x}\text{R}_x\text{Fe}_2\text{As}_2$ series, the 20 K phase may be related to another strain-induced phase that is well documented in the case of SrFe_2As_2 [39] to be driven by lattice distortions induced by strained sample conditions.

Because relatively high pressures are needed to achieve the range where these transitions appear, it is possible that a transition to the collapsed tetragonal (cT) phase occurs in this region. Nevertheless, the sudden appearance of superconductivity with the loss of AFM order in a pressure window of less than 2 kbar indicates the mutually exclusive nature of the two phases. This is strikingly similar to that observed in 1111 iron-based superconductors, where the two phases compete for the ground state [6,7]. Furthermore, it also confirms that the trace high- T_c phase is highly unlikely to be extrinsic in origin, as recently suggested to originate from structural clustering [54] that would presumably exhibit a signature in resistivity at all pressures and not onset upon pressure increase, as observed here. Rather, this must be an intrinsic phenomenon stabilized by rare-earth substitution and/or the suppression of AFM order. This issue is expounded upon in Sec. IV. The role of nonhydrostaticity on this phenomenon is considered next.

B. Hydrostatic helium cell

1. Neutron experiment

To further clarify the interplay of AFM and high- T_c superconductivity, we investigated the magnetic properties of another underdoped sample with a lower $T_N(0)$ (i.e., closer to the border of the SC dome) under hydrostatic pressure in a helium pressure cell. Neutron diffraction experiments were carried out on sample S2 [$x = 0.12$, $T_N(0) = 70$ K] under applied He gas pressure, allowing determination of both the magnetic and structural phases directly. Figure 3 presents the normalized data and fits to the integrated intensities for a few selected pressures. An example of the scattering intensity as a function of temperature and diffraction angle is presented as a contour plot in Fig. 4(a). This intensity is proportional to the square of the staggered magnetization, or AFM order parameter, as plotted in Fig. 3 along with mean-field fits. The resultant fit estimates of $T_N(P)$ are summarized in Fig. 4(a) as a function of pressure. The value of $T_N(0) = 70$ K at ambient pressure [Fig. 3(a)] is consistent with that determined by the drop in the magnetic susceptibility (not shown; see the supplemental material [43]).

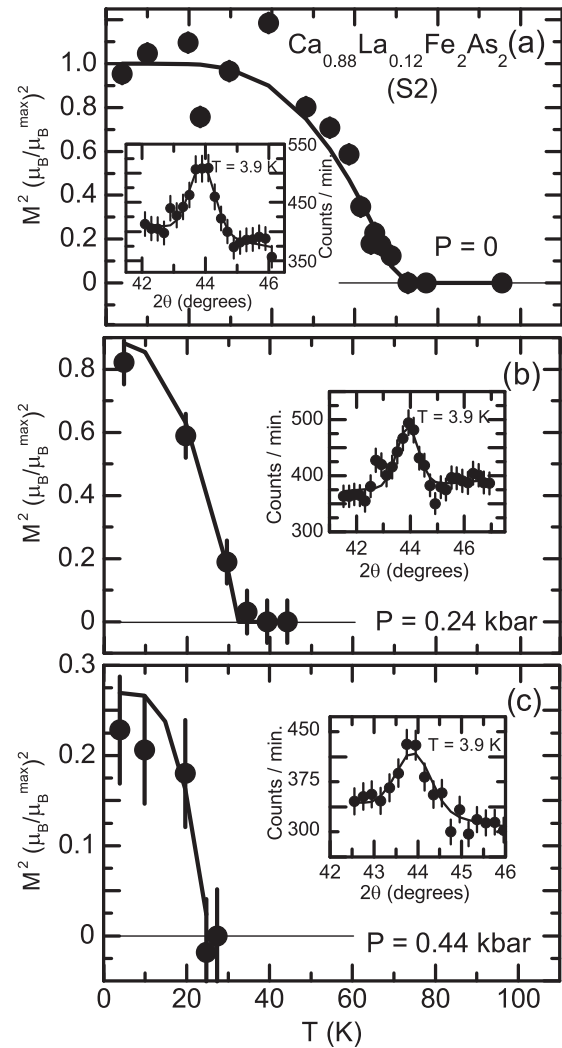


FIG. 3. Hydrostatic pressure dependence of ordered AFM moments in $\text{Ca}_{0.88}\text{La}_{0.12}\text{Fe}_2\text{As}_2$ (underdoped sample “S2” in Fig. 1) determined by neutron scattering experiments on the BT-4 beam line at the NCNR. Integrated intensities measured at the $Q_{\text{AFM}} = (1\ 0\ 3)$ magnetic Bragg peak are shown for selected applied pressures of (a) $P = 0$, (b) $P = 0.24$ kbar, and (c) $P = 0.44$ kbar. Intensities are proportional to the square of the magnetic order parameter M^2 , which is the ordered moment at (P, T) . Values are normalized to the maximum ambient pressure value observed at 3.9 K. Solid lines are mean-field order fits to M^2 to obtain the Néel temperatures for each pressure. Insets show data from θ - 2θ scans at 3.9 K, fit to a Gaussian line shape with a sloping background.

As shown in Fig. 3, the value of $T_N(P)$ is dramatically suppressed with increasing hydrostatic pressure, with no magnetic peak detectable at 0.55 kbar pressure down to 4 K (not shown). This rate of suppression, $dT_N/dP \simeq -125$ K/kbar, is profoundly different from that found in the quasi-hydrostatic clamp cell experiment presented in Fig. 2, where $dT_N/dP \simeq -4.7$ K/kbar is approximately 25 times smaller. It is in fact comparable to the largest reported pressure coefficient $dT_N/dP \simeq -110$ K/kbar reported in $\text{Ca}(\text{Fe}_{1-x}\text{Co}_x)_2\text{As}_2$ under hydrostatic pressure [44].

The reason for such dramatic differences in pressure dependence is debatable. It is certainly likely that dT_N/dP

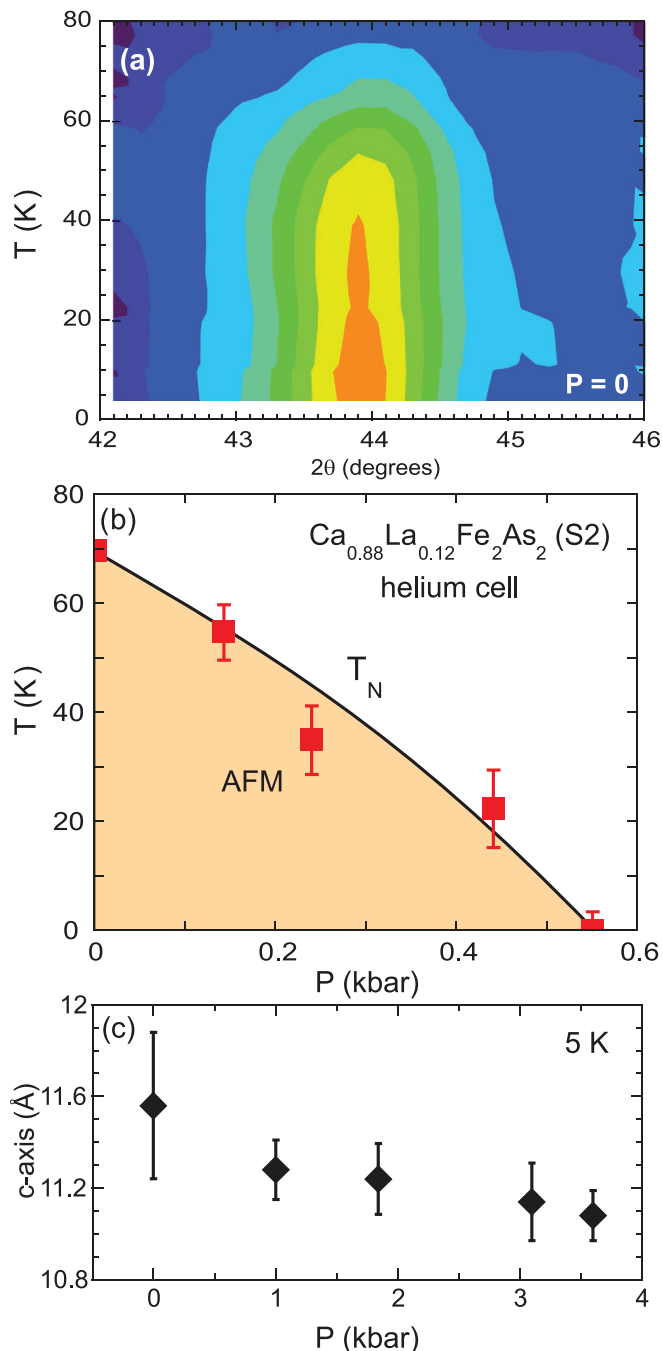


FIG. 4. (Color online) (a) Magnetic intensity of the (1 0 3) Bragg peak at ambient pressure in $\text{Ca}_{0.88}\text{La}_{0.12}\text{Fe}_2\text{As}_2$ (underdoped sample “S2” in Fig. 1) determined from neutron diffraction on the BT-4 beamline at the NCNR. (b) Hydrostatic pressure dependence of T_N in $\text{Ca}_{0.88}\text{La}_{0.12}\text{Fe}_2\text{As}_2$ determined by magnetic order parameter fits (see Fig. 3). (c) Variation of the c -axis lattice parameter vs pressure determined by measuring the (0 0 4) structural Bragg reflection at 5 K. Uncertainties are statistical in origin and represent one standard deviation.

is a nonlinear parameter that is strongly dependent on the rare-earth concentration (and thus depends very sensitively on small changes in lattice parameters, since La substitution does not introduce significant changes to the unit cell [28]). The degree of pressure homogeneity is certainly a factor,

and the Poisson effect due to anisotropic change of lattice parameters under inhomogeneous pressure combined with an anisotropic pressure transmission from a frozen pressure medium could possibly lead to such differences. In any case, it is well established that the CaFe_2As_2 system is extremely sensitive to the nature of structural perturbation caused by chemical or applied pressure application due to its proximity to a structural instability that drives a change in the bonding structure in the ThCr_2Si_2 -type unit cell. The proximity of interlayer As-As dimer formation to the range of unit cell parameters encountered upon moderate tuning of CaFe_2As_2 changes the bonding structure of the crystal in a very abrupt structural collapse of the unit cell [28,36,46] that occurs midway through the AFM-SC phase diagram of the undoped system, amplifying the effects of strain induced by nonhydrostatic pressure conditions.

Neutron and x-ray scattering and transport studies in CaFe_2As_2 under hydrostatic pressure have shown that T_N is rapidly suppressed, and at a pressure of 3.5 kbar the system undergoes another dramatic structural phase transition into the cT phase [36,46]. To determine the possible proximity of the pressure-induced collapse transition in our pressure experiments, measurements of the c -axis lattice parameter were obtained up to 3.6 kbar at 5 K. As shown in Fig. 4(c), the variation of the c -axis lattice parameter with pressure exhibits no significant change with pressure, demonstrating the absence of any structural collapse up to at least ~ 4 kbar. However, the obvious sensitivity of both the magnetic and structural stability of the $\text{Ca}_{1-x}\text{R}_x\text{Fe}_2\text{As}_2$ system to the nature of applied strain suggests that all physical properties, including the appearance of superconducting phases, are strongly coupled to the delicate structural instabilities in this system.

2. Resistivity experiment

In a separate He-gas pressure experiment, resistivity of a sample even closer to the SC-AFM boundary was measured in a hydrostatic helium cell at McMaster University. Figure 5(a) presents the temperature dependence of the resistance of sample S3 [$x = 0.13$, $T_N(0) = 58$ K] for a series of applied pressures. At ambient pressure, the resistivity of this sample exhibits an upturn upon decreasing temperature at 58 K, as determined by a change in $d\rho/dT$ (see the supplemental material [43]); we use this to define $T_N(0) = 58$ K as the AFM transition (consistent with that used above for sample S1). At lower temperatures, there is a sharp drop of resistance due to the “10 K” superconducting transition at $T_{c1} = 10$ K, as also observed in sample S1 (see Fig. 2). With increasing pressure, T_N shifts to lower temperatures as indicated by the positions of the down arrows, demonstrating a rapid suppression of magnetic order. At only 50 bar, T_N decreases to ~ 40 K, yielding a pressure coefficient $dT_N/dP \sim -350$ K/kbar. This is even more dramatic than that found in the neutron experiment above for sample S2, where $dT_N/dP \simeq -125$ K/kbar, suggesting that a nonlinear dependence of the rate of change of T_N with pressure on rare-earth concentration is certainly present. However, the focus of this study, namely the high- T_c superconducting phase, suggests that its sensitivity to differing pressure conditions is not nearly as dramatic, as discussed in the next section.

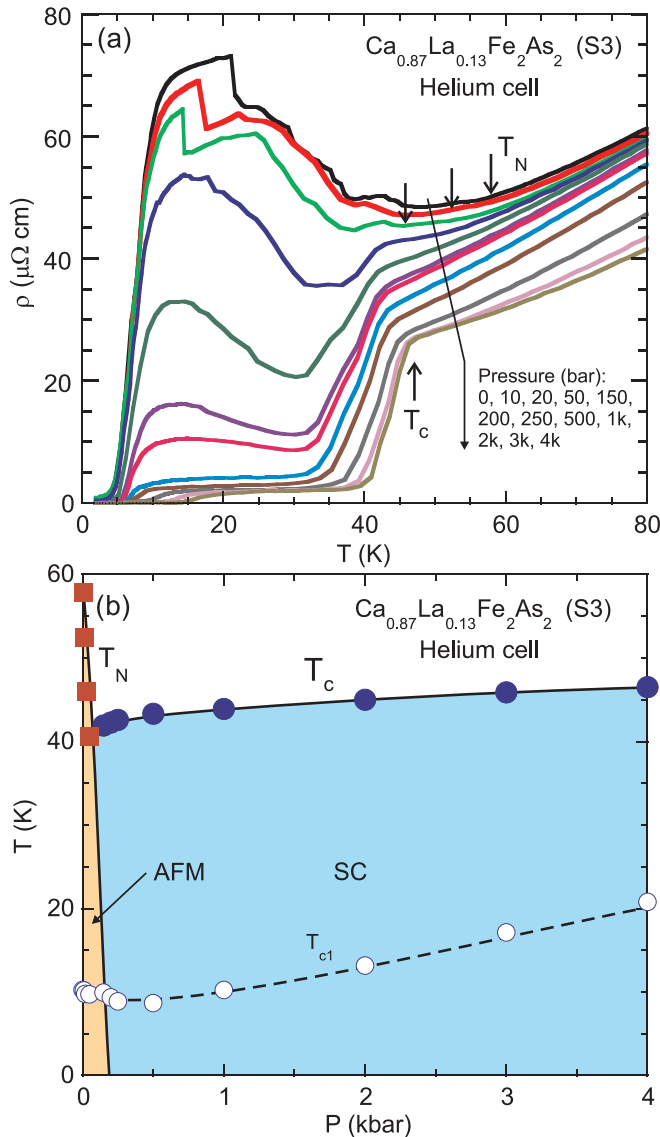


FIG. 5. (Color online) Hydrostatic pressure dependence of electrical resistivity of $\text{Ca}_{0.87}\text{La}_{0.13}\text{Fe}_2\text{As}_2$ (underdoped sample “S3” in Fig. 1) using helium gas as the pressure medium. (a) Resistivity temperature dependence as a function of applied pressures. Down arrows mark the antiferromagnetic ordering transition temperature T_N for each pressure, as determined by $d\rho/dT$ analysis (see text), and the up arrow indicates an example of the onset of superconductivity at T_c for the sample under 4 kbar pressure. (b) Temperature vs hydrostatic pressure phase diagram of antiferromagnetic (squares) and superconducting transition temperatures T_c (solid circles) and T_{c1} (open circles).

At $P = 50$ bar, an abrupt drop in resistance begins to appear, consistent with the onset of high- T_c superconductivity at 40 K. Upon further pressure increase, the drop develops to an almost complete resistive transition with onset temperature at 46.5 K and no trace of the AFM resistance minimum. The results shown in Fig. 5 set an upper bound of ~ 0.25 kbar under hydrostatic pressure for the coexistence between the AFM and high- T_c SC phases, if they coexist at all. This high- T_c SC phase reaches its maximum $T_c = 46.5$ K at 4 kbar. The resistivity not reaching zero below the high- T_c SC transition indicates partial

volume fraction superconductivity as studied previously [28], which remains unexplained. At the disappearance of T_N , the T_{c1} phase is enhanced with pressure, reaching a maximum value of $T_{c1} \simeq 20$ K at 4 kbar.

The incredibly small pressure scales used in this experiment (for instance, beginning at 10 bar or ~ 10 atmospheres of pressure) to induce rather large changes in transport properties are strongly suggestive that the application of pressure does not induce any irreversible pressure or strain effect that may lead to an extrinsic phase. Also, note that this transformation cannot originate from a transition to the cT phase, as demonstrated by the neutron experiment lattice parameter study presented in Fig. 3(c). Rather, this abrupt appearance of the high- T_c transition coincident with the suppression of AFM order again confirms the intrinsic origin of this superconducting phase and its exclusive existence.

The apparent coexistence of the high- T_c superconductivity and the AFM in an extremely narrow pressure window (≤ 0.2 kbar) is similar to what was also found in the 1111 family of superconductors by μSR experiments [8], which is a very sensitive bulk probe. Interestingly, a similar phenomenon was also observed in the closely related system $\text{Ca}(\text{Fe}_{1-x}\text{Co}_x)_2\text{As}_2$, where AFM order is also suppressed with extremely small hydrostatic pressures in annealed samples with reduced T_N values to reveal a superconducting phase that shows no coexistence with the AFM phase [44]. Gati *et al.* have ascribed this behavior to a strong first-order character of the magnetostructural transition. While it is not clear that the $\text{Ca}_{1-x}\text{La}_x\text{Fe}_2\text{As}_2$ series entails as strong a first-order character (for instance, as shown by the order parameter temperature dependence presented in Fig. 3), it is true that the magnetostructural transition in the 122 series becomes much more first-order in nature toward the Ca end member [45]. Future studies should help determine if this feature is a common tie between the exclusivity of AFM and SC phases found in the two Ca-based 122 systems.

C. Moissanite anvil cell

To understand the response of superconductivity in “overdoped” samples to pressure, we have investigated overdoped sample S4 [$x = 0.27$, $T_c(0) = 31$ K] in the higher quasi-hydrostatic pressure range using an anvil cell technique. Figure 6(a) presents the temperature dependence of the TDO frequency at various pressures with the background removed. The background is determined by a linear extrapolation of the data above the superconducting transition to the lowest temperature of a particular run, as depicted in the upper inset to Fig. 6(a). The data are plotted as $-1 \times$ frequency, so that the superconducting transition appears as a drop in order to facilitate easy comparison with resistivity data. We determine T_c by the intersection of two lines as shown in the main panel of Fig. 6(a). Resistance measurements on a similar sample S4’ were performed using a miniature piston-cylinder clamp cell (similar to that used for sample S1) to compare the effects of slightly different quasi-hydrostatic pressure conditions on an overdoped concentration, with complete resistive transitions presented in Fig. 6(b).

Using the data from both TDO and resistivity measurements, the pressure-temperature phase diagram for overdoped

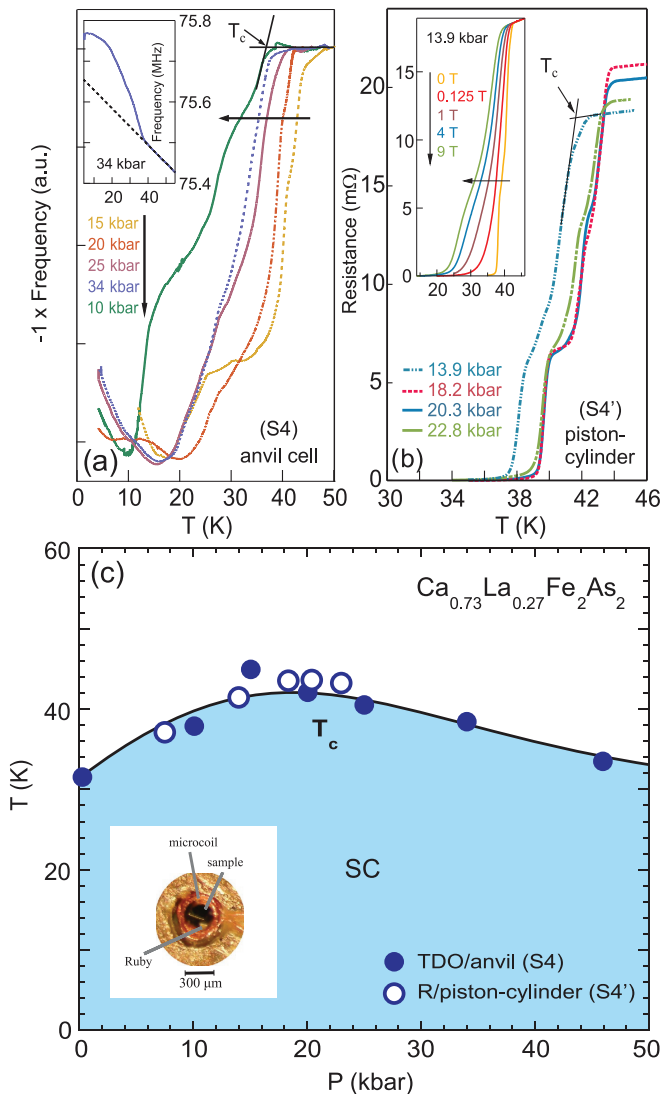


FIG. 6. (Color online) Pressure dependence of superconducting transition of $\text{Ca}_{0.73}\text{La}_{0.27}\text{Fe}_2\text{As}_2$ (overdoped sample “S4” in Fig. 1). (a) Temperature dependence of the tunnel diode oscillator frequency of single-crystal sample S4 at various applied pressures obtained using a Moissanite anvil cell (note: the sign of the vertical axis has been inverted). Inset: example of raw data and background estimation (see text). (b) Electrical resistance of sample S4 measured using a piston-cylinder cell. Inset: magnetic-field dependence of the superconducting transition at 13.9 kbar applied pressure. (c) Phase diagram showing the pressure dependence of the superconducting transition for samples S4 (closed circles) and S4’ (open circles) as shown in panels (a) and (b), respectively. The solid curve is a guide to the eye. Inset: photograph of TDO measurement setup, with a 10-turn microcoil with a diameter of 300 μm enclosing the sample and a ruby chip used for pressure determination.

samples S4 and S4’ has been constructed as shown in Fig. 6(c). As shown, the SC transition temperature rises from 31 K at ambient pressure to a maximum value of ~ 44 K at 20 kbar, before decreasing slightly at higher pressures. The anvil and clamp cell experiments compare favorably, with T_c values that closely follow each other, indicating little to no sensitivity of the overdoped T_c pressure dependence on hydrostaticity

of applied pressure. The increase in T_c follows an average slope of $\sim +0.65$ K/kbar, a value that is considerably higher than other electron-doped 122 pnictides. In overdoped $\text{BaFe}_{1.8}\text{Co}_{0.2}\text{Fe}_2\text{As}_2$, for example, T_c was observed to increase with an initial slope of 0.065 K/kbar [47] and then level off at higher pressures where T_c increases only 1 K when applying 25 kbar. In the underdoped regime, on the other hand, the pressure coefficient does become sizable, reaching 0.4 K/kbar for a sample with composition $\text{BaFe}_{1.92}\text{Co}_{0.08}\text{Fe}_2\text{As}_2$ [47]. The clear maximum in T_c versus pressure raises the question as to why an overdoped sample of $\text{Ca}_{1-x}\text{La}_x\text{Fe}_2\text{As}_2$ displays the pressure sensitivity characteristic of an underdoped sample of $\text{BaFe}_{2-x}\text{Co}_x\text{As}_2$. From a structural perspective, the replacement of Ca (atomic radius 126 pm) with La (130 pm) expands the a -axis lattice parameter, from 3.895 Å for pure CaFe_2As_2 to 3.92 Å for $x = 0.27$ as measured at 250 K. The c -axis lattice parameter remains essentially unchanged within the margins of error in the measurement [28]. Applying hydrostatic pressure to CaFe_2As_2 has a somewhat different effect, causing a significant shortening of the c axis, from 11.75 to 11.50 Å by 10 kbar in the high-temperature tetragonal phase (T') at room temperature. Over the same pressure range, the a -axis lattice constant increases slightly, by 0.1% [48]. However, it is quite interesting to note that the maximum value of $T_c = 44$ K seen in our pressure experiments on both underdoped and overdoped $\text{Ca}_{1-x}\text{La}_x\text{Fe}_2\text{As}_2$ samples is very close to that seen at ambient pressure in optimally doped $\text{Ca}_{0.8}\text{La}_{0.2}\text{Fe}_2\text{As}_2$ (maximum $T_c = 43$ K) [28,29].

Alternatively, one might consider the role of density fluctuations in boosting T_c . For undoped CaFe_2As_2 at room temperature, a volume collapse into the cT state is known to occur when the interlayer As-As separation approaches 3.0 Å [28,46]. At sufficiently high pressures, it is possible that a cT transition may be induced, as was found in $\text{Ca}_{0.67}\text{Sr}_{0.33}\text{Fe}_2\text{As}_2$ [49].

It is interesting to compare these findings with recent experiments on phosphorus co-doping in the rare-earth substituted CaFe_2As_2 system [34]. Isovalent substitution of P for As ions in the $\text{Ca}_{1-x}\text{La}_x\text{Fe}_2(\text{As}_{1-y}\text{P}_y)_2$ appears to create an island of high volume fraction superconductivity, for samples close to the doping levels $x = 0.12$ and $y = 0.06$. In some pnictides, such as the $\text{BaFe}_2(\text{As}_{1-x}\text{P}_x)_2$ system, the equivalence of P substitution and pressure has been established [50]. Given this result, it seems interesting to probe the superconducting volume fraction in our system of samples with La doping $x = 0.12$ under hydrostatic pressure, to see whether a similar island of optimized superconductivity occurs.

IV. GENERAL DISCUSSION

Considering that isovalent P substitution in $\text{CaFe}_2\text{As}_{2-x}\text{P}_x$ also induces the structural collapse without a high- T_c phase present [51], it appears that charge doping is an essential ingredient for the high- T_c superconducting phase to stabilize [28]. In $\text{Ca}_{1-x}\text{R}_x\text{Fe}_2\text{As}_2$, one proposed scenario is that the low-volume-fraction high- T_c phase might be inhomogeneous, originating from local effects tied to the low percentage of rare-earth substitution. However, recent STM measurement on $\text{Ca}_{1-x}\text{Pr}_x\text{Fe}_2\text{As}_2$ demonstrated that Pr dopants do not cluster [52], as is found in other substitution systems (e.g.,

$\text{Sr}_{1-x}\text{K}_x\text{Fe}_2\text{As}_2$ [53]), and in fact show a slight tendency to repel each other at very short length scales. These findings suggest that Pr inclusion or its inhomogeneous distribution is unlikely to be the source of the high- T_c phase [52], similar to what has been concluded in the case of $R\text{FeAsO}_{1-x}\text{F}_x$, where neutron studies that distinguish between a magnetic Kramers doublet ground state for $R = \text{Nd}$ and a singlet state for $R = \text{Pr}$ rule out any direct role of R substitution for the high- T_c phase [19].

It has been suggested that interfacial superconductivity is the mechanism driving the high- T_c phase [54]. In this scenario, superconductivity is occurring at the interface of small clusterlike regions elongated along the ab plane inside the bulk metallic region. However, the pressure-driven superconductivity observed in the current study does not support the scenario in which intergrowth or cluster regions are responsible for the trace high- T_c superconductivity. More importantly, the recent observation of much greater volume fractions of superconductivity in phosphorus-substituted samples [34] is also inconsistent with such a scenario.

Rather, our study strongly indicates that long-range magnetic order must be fully suppressed in order to induce the high- T_c superconducting phase. If cluster or interface regions play any role in stabilizing the high- T_c phase, they must also abruptly appear beyond the AFM-SC transition. Given the vastly different rates of suppression of T_N with pressure in nonhydrostatic (Fig. 2) and hydrostatic (Fig. 4) pressure experiments, it is highly unlikely that such regions form equivalently under dramatically different strain conditions. It is clear that lattice strain, and the resultant local perturbations on electronic and magnetic structure, must play a key role in stabilizing the superconducting phase, as is well documented in the case of SrFe_2As_2 [39], where lattice distortions are directly tied to the appearance of superconductivity.

Recently, superconductivity at 45 K has been reported in $\text{Ca}_{1-x}\text{La}_x\text{FeAs}_2$, a “112”-type (space group P21) variation of the 122 compound studied here, but with a monoclinic structural distortion [55,56]. Because the Meissner screening fractions reported for the 112 phase are sizable ($\sim 80\%$), it is tempting to assign traces of high- T_c superconductivity in the 122 system to impurity-type inclusions of this new phase. However, we note that this phase is as unlikely as the “structural cluster” scenario proposed in Ref. [54] for the same reasons presented above. Furthermore, extensive single-crystal x-ray diffraction investigations [28] have found no detectable trace of the 112 phase in 122 samples. In fact, the report of large volume fraction Meissner screening in the 112 phase is similar to that reported by the same authors for phosphorus-substituted 122 samples [34], suggesting the possibility of high- T_c superconductivity is intrinsic to both of these structures and not limited to one or the other.

Finally, the most striking observations in the $\text{Ca}_{1-x}\text{R}_x\text{Fe}_2\text{As}_2$ series involve the scale of the superconducting temperature, reaching near 50 K and approaching that of the highest- T_c oxypnictide 1111 compounds. It is striking that, both in the 1111 materials and in the 122 system considered here, the temperature-doping phase diagrams include a strong segregation between AFM and SC phases with little to no coexistence. (Although coexistence has indeed been observed in the $\text{SmFeAsO}_{1-x}\text{F}_x$ system [57], it is widely thought

to originate from a percolative-type segregation of AF and paramagnetic-metal domains [20] that results in the observed phase separation [58].) It is thus tempting to draw parallels between the origin of the highest- T_c pairing that may be common in the two systems, given these similarities. First, the first-order nature of the separation between AFM and SC phases may have roots in the interplay between magnetic and structural (nematic) instabilities that impinge on the superconducting phase. Theoretical work by Fernandes *et al.* has recently shown that the presence of superconductivity has a profound effect on the first-order character of the phase transition between AFM and paramagnetic/superconducting phases [17], which in the limit of large Fermi surface nesting mismatch drives away the coexistence of the two phases. Why T_c is maximized in such systems remains to be understood, but the complete separation of AFM and SC phases is likely to play a role, perhaps due to a lack of anisotropy in the superconducting gap that can derive from the presence of Fermi surface reconstruction in the spin-density wave state [59,60]. Most recently, the emergence of two superconducting domes in the phase diagram of $\text{LaFeAsO}_{1-x}\text{H}_x$ [61] is a tantalizing hint at the possibility of two distinct superconducting phases that may find a basis in these closely related but distinct iron-based materials.

In summary, we have employed both quasihydrostatic and hydrostatic pressures to illuminate the pressure-temperature phase diagrams of underdoped $\text{Ca}_{1-x}\text{La}_x\text{Fe}_2\text{As}_2$ as well as the quasihydrostatic pressure dependence of an overdoped sample of $\text{Ca}_{1-x}\text{La}_x\text{Fe}_2\text{As}_2$ with $x = 0.27$. Interestingly, high-temperature superconductivity in the $\text{Ca}_{1-x}\text{R}_x\text{Fe}_2\text{As}_2$ series appears after the complete suppression of the AFM phase, with little or no coexistence between the two phases. This is strikingly similar to the segregation of SC and AFM phases found in 1111 materials doped with fluorine, such as in $\text{LaFeAsO}_{1-x}\text{F}_x$ [7], $\text{CeFeAsO}_{1-x}\text{F}_x$ [6], and $\text{SmFeAsO}_{1-x}\text{F}_x$ [8], and it should be contrasted with the well-known coexistence shown to occur in $\text{BaFe}_{2-x}\text{Co}_x\text{As}_2$ [9,10,50]. Complete suppression of magnetic order appears to be a necessary condition for the high- T_c superconductivity, as in the case of the 1111 family. In the overdoped sample, a rapid rise in T_c , where one might naively expect suppression, suggests that the application of pressure in this system does not simply follow the expectation from doping, and offers an additional route to tune T_c in this family of materials. Above all, in contrast to the lower- T_c systems where usually superconductivity and magnetism happily coexist, the tendency for the highest- T_c systems to show no coexistence of the two phases provides an important clue to the pairing mechanism in iron-based superconductors.

ACKNOWLEDGMENTS

The authors acknowledge R. L. Greene, P. Canfield, G. Lonzarich, and P. Alireza for useful discussions, and we thank J. Leao for assistance with neutron diffraction measurements under pressure. Research at the University of Maryland was supported by the AFOSR-MURI (FA9550-09-1-0603) and the NSF (DMR-0952716). M.S. acknowledges support from the Royal Society, and S.K.G. from Trinity College Cambridge.

- [1] Y. Kamihara, T. Watanabe, M. Hirano, and H. Hosono, *J. Am. Chem. Soc.* **130**, 3296 (2008).
- [2] J. Paglione and R. L. Greene, *Nat. Phys.* **6**, 645 (2010).
- [3] D. C. Johnston, *Adv. Phys.* **59**, 803 (2010).
- [4] G. R. Stewart, *Rev. Mod. Phys.* **83**, 1589 (2011).
- [5] Z.-A. Ren, W. Lu, J. Yang, W. Yi, X.-L. Shen, Z. Cai, G.-C. Che, X.-L. Dong, L.-L. Sun, F. Zhou, and Z.-X. Zhao, *Chin. Phys. Lett.* **25**, 2215 (2008).
- [6] H. Luetkens *et al.*, *Nat. Mater.* **8**, 305 (2009).
- [7] J. Zhao, Q. Huang, C. d. I. Cruz, S. Li, J. W. Lynn, Y. Chen, M. A. Green, G. F. Chen, G. Li, Z. Li, J. L. Luo, N. L. Wang, and P. Dai, *Nat. Mat.* **7**, 953 (2008).
- [8] H. Maeter *et al.*, [arXiv:1210.6959](https://arxiv.org/abs/1210.6959).
- [9] N. Ni, M. E. Tillman, J.-Q. Yan, A. Kracher, S. T. Hannahs, S. L. Budko, and P. C. Canfield, *Phys. Rev. B* **78**, 214515 (2008).
- [10] J.-H. Chu, J. G. Analytis, C. Kucharczyk, and I. R. Fisher, *Phys. Rev. B* **79**, 014506 (2009).
- [11] D. K. Pratt, W. Tian, A. Kreyssig, J. L. Zarestky, S. Nandi, N. Ni, S. L. Budko, P. C. Canfield, A. I. Goldman, and R. J. McQueeney, *Phys. Rev. Lett.* **103**, 087001 (2009).
- [12] M.-H. Julien, H. Mayaffre, M. Horvatic, C. Berthier, X. D. Zhang, W. Wu, G. F. Chen, N. L. Wang, and J. L. Luo, *Europhys. Lett.* **87**, 37001 (2009).
- [13] Z. Li, R. Zhou, Y. Liu, D. L. Sun, J. Yang, C. T. Lin, and G.-q. Zheng, *Phys. Rev. B* **86**, 180501(R) (2012).
- [14] Y. Laplace, J. Bobroff, F. Rullier-Albenque, D. Colson, and A. Forget, *Phys. Rev. B* **80**, 140501(R) (2009).
- [15] S. Ran, S. L. Budko, W. E. Straszheim, J. Soh, M. G. Kim, A. Kreyssig, A. I. Goldman, and P. C. Canfield, *Phys. Rev. B* **85**, 224528 (2012).
- [16] R. M. Fernandes, D. K. Pratt, W. Tian, J. Zarestky, A. Kreyssig, S. Nandi, M. G. Kim, A. Thaler, N. Ni, P. C. Canfield, R. J. McQueeney, J. Schmalian, and A. I. Goldman, *Phys. Rev. B* **81**, 140501(R) (2010).
- [17] R. M. Fernandes, S. Maiti, P. Wölfle, and A. V. Chubukov, *Phys. Rev. Lett.* **111**, 057001 (2013).
- [18] R. M. Fernandes and J. Schmalian, *Phys. Rev. B* **82**, 014521 (2010).
- [19] E. A. Goremychkin *et al.*, *Phys. Rev. B* **83**, 212505 (2011).
- [20] N. Fujiwara, T. Nakano, Y. Kamihara, and H. Hosono, *Phys. Rev. B* **85**, 094501 (2012).
- [21] N. Kumar, R. Nagalakshmi, R. Kulkarni, P. L. Paulose, A. K. Nigam, S. K. Dhar, and A. Thamizhavel, *Phys. Rev. B* **79**, 012504 (2009).
- [22] N. Kumar, S. Chi, Y. Chen, K. G. Rana, A. K. Nigam, A. Thamizhavel, W. Ratcliff, S. K. Dhar, and J. W. Lynn, *Phys. Rev. B* **80**, 144524 (2009).
- [23] K. Zhao, Q. Q. Liu, X. C. Wang, Z. Deng, Y. X. Lv, J. L. Zhu, F. Y. Li, and C. Q. Jin, *J. Phys.: Condens. Matter* **22**, 222203 (2010).
- [24] M. S. Torikachvili, S. L. Budko, N. Ni, and P. C. Canfield, *Phys. Rev. Lett.* **101**, 057006 (2008).
- [25] T. Park, E. Park, H. Lee, T. Klimczuk, E. D. Bauer, F. Ronning, and J. D. Thompson, *J. Phys.: Condens. Matter* **20**, 322204 (2008).
- [26] P. L. Alireza, Y. T. C. Ko, J. Gillett, C. M. Petrone, J. M. Cole, G. G. Lonzarich, and S. E. Sebastian, *J. Phys.: Condens. Matter* **21**, 012208 (2009).
- [27] W. Yu, A. A. Aczel, T. J. Williams, S. L. Budko, N. Ni, P. C. Canfield, and G. M. Luke, *Phys. Rev. B* **79**, 020511(R) (2009).
- [28] S. R. Saha, N. P. Butch, T. Drye, J. Magill, S. Ziemak, K. Kirshenbaum, P. Y. Zavalij, J. W. Lynn, and J. Paglione, *Phys. Rev. B* **85**, 174524 (2012).
- [29] Z. Gao, Y. Qi, L. Wang, D. Wang, X. Zhang, C. Yao, C. Wang, and Y. Ma, *Europhys. Lett.* **95**, 67002 (2011).
- [30] B. Lv, L. Denga, M. Goocha, F. Weia, Y. Suna, J. K. Meena, Y.-Y. Xuea, B. Lorenza, and C.-W. Chu, *Proc. Natl. Acad. Sci. (USA)* **108**, 15705 (2011).
- [31] M. Rotter, M. Tegel, and D. Johrendt, *Phys. Rev. Lett.* **101**, 107006 (2008).
- [32] J. Nagamatsu, N. Nakagawa, T. Muranaka, Y. Zenitani, and J. Akimitsu, *Nature (London)* **410**, 63 (2001).
- [33] T. Drye, S. R. Saha, J. Paglione, and P. Y. Zavalij, *Supercond. Sci. Technol.* **25**, 084014 (2012).
- [34] K. Kudo, K. Iba, M. Takasuga, Y. Kitahama, J.-I. Matsumura, M. Danura, Y. Nogami, and M. Nohara, *Sci. Rep.* **3**, 1478 (2013).
- [35] T. Yildirim, *Phys. Rev. Lett.* **102**, 037003 (2009).
- [36] A. I. Goldman, A. Kreyssig, K. Proke, D. K. Pratt, D. N. Argyriou, J. W. Lynn, S. Nandi, S. A. J. Kimber, Y. Chen, Y. B. Lee, G. Samolyuk, J. B. Leao, S. J. Poulton, S. L. Budko, N. Ni, P. C. Canfield, B. N. Harmon, and R. J. McQueeney, *Phys. Rev. B* **79**, 024513 (2009).
- [37] H. Gretarsson, S. R. Saha, T. Drye, J. Paglione, J. Kim, D. Casa, T. Gog, W. Wu, S. R. Julian, and Y.-J. Kim, *Phys. Rev. Lett.* **110**, 047003 (2013).
- [38] L. Ma, G. F. Ji, J. Dai, S. R. Saha, J. Paglione, and W. Yu, *Chin. Phys. B* **22**, 057401 (2013).
- [39] S. R. Saha, N. P. Butch, K. Kirshenbaum, J. Paglione, and P. Y. Zavalij, *Phys. Rev. Lett.* **103**, 037005 (2009).
- [40] H. Xiao, T. Hu, A. P. Dioguardi, N. Roberts-Warren, A. C. Shockley, J. Crocker, D. M. Nisson, Z. Viskadourakis, X. Tee, I. Radulov, C. C. Almasan, N. J. Curro, and C. Panagopoulos, *Phys. Rev. B* **85**, 024530 (2012).
- [41] S. R. Saha, H. Sugawara, T. Namiki, Y. Aoki, and H. Sato, *Phys. Rev. B* **65**, 214429 (2002), and references therein.
- [42] S. K. Goh, Y. Nakai, K. Ishida, L. E. Klintberg, Y. Ihara, S. Kasahara, T. Shibauchi, Y. Matsuda, and T. Terashima, *Phys. Rev. B* **82**, 094502 (2010).
- [43] See Supplemental Material at <http://link.aps.org/supplemental/10.1103/PhysRevB.89.134516> for more information about the determination of T_N .
- [44] E. Gati, S. Köhler, D. Guterding, B. Wolf, S. Knöner, S. Ran, S. L. Bud'ko, P. C. Canfield, and M. Lang, *Phys. Rev. B* **86**, 220511 (2012).
- [45] K. Kirshenbaum, N. P. Butch, S. R. Saha, P. Y. Zavalij, B. G. Ueland, J. W. Lynn, and J. Paglione, *Phys. Rev. B* **86**, 060504(R) (2012).
- [46] A. Kreyssig, M. A. Green, Y. Lee, G. D. Samolyuk, P. Zajdel, J. W. Lynn, S. L. Budko, M. S. Torikachvili, N. Ni, S. Nandi, J. B. Leao, S. J. Poulton, D. N. Argyriou, B. N. Harmon, R. J. McQueeney, P. C. Canfield, and A. I. Goldman, *Phys. Rev. B* **78**, 184517 (2008).
- [47] K. Ahilan, F. L. Ning, T. Imai, A. S. Sefat, M. A. McGuire, B. C. Sales, and D. Mandrus, *Phys. Rev. B* **79**, 214520 (2009).

- [48] P. Canfield, S. Budko, N. Nia, A. Kreyssig, A. Goldman, R. McQueeney, M. Torikachvili, D. Argyriou, G. Luke, and W. Yu, *Physica C* **469**, 404 (2009).
- [49] J. R. Jeffries, N. P. Butch, K. Kirshenbaum, S. R. Saha, G. Samudrala, S. T. Weir, Y. K. Vohra, and J. Paglione, *Phys. Rev. B* **85**, 184501 (2012).
- [50] L. E. Klintberg, *J. Phys. Soc. Jpn.* **79**, 123706 (2010).
- [51] S. Kasahara, T. Shibauchi, K. Hashimoto, Y. Nakai, H. Ikeda, T. Terashima, and Y. Matsuda, *Phys. Rev. B* **83**, 060505 (2011).
- [52] I. Zeljkovic, D. Huang, C.-L. Song, B. Lv, C.-W. Chu, and J. E. Hoffman, *Phys. Rev. B* **87**, 201108(R) (2013).
- [53] C.-L. Song, Y. Yin, M. Zech, T. Williams, M. M. Yee, G.-F. Chen, J.-L. Luo, N.-L. Wang, E. W. Hudson, and J. E. Hoffman, *Phys. Rev. B* **87**, 214519 (2013).
- [54] F. Y. Wei *et al.*, [arXiv:1309.0034](https://arxiv.org/abs/1309.0034).
- [55] N. Katayama, K. Kudo, S. Onari, T. Mizuaki, K. Sugawara, Y. Sugiyama, Y. Kitaham, K. Iba, K. Fujimura, N. Nishimoto, M. Nohara, and H. Sawa, *J. Phys. Soc. Jpn.* **82**, 123702 (2013).
- [56] K. Kudo, T. Mizukami, Y. Kitahama, D. Mitsuoka, K. Iba, K. Fujimura, N. Nishimoto, Y. Hiraoka, and M. Nohara, *J. Phys. Soc. Jpn.* **83**, 025001 (2014).
- [57] A. J. Drew *et al.*, *Nat. Mater.* **8**, 310 (2009).
- [58] G. Prando, S. Sanna, G. Lamura, T. Shiroka, M. Tropeano, A. Palenzona, H.-J. Grafe, B. Büchner, P. Carretta, and R. De Renzi, *Phys. Status Solidi* **250**, 599 (2013).
- [59] S. Maiti, R. M. Fernandes, and A. V. Chubukov, *Phys. Rev. B* **85**, 144527 (2012).
- [60] J.-Ph. Reid *et al.*, *Phys. Rev. B* **82**, 064501 (2010).
- [61] N. Fujiwara, S. Tsutsumi, S. Iimura, S. Matsuishi, H. Hosono, Y. Yamakawa, and H. Kontani, *Phys. Rev. Lett.* **111**, 097002 (2013).